Characterization of Photoelectrocatalytic Processes at Nanoporous TiO_2 Film Electrodes: Photocatalytic Oxidation of Glucose

Dianlu Jiang, Huijun Zhao,* Shanqing Zhang, and Richard John

School of Environmental and Applied Sciences, Gold Coast Campus, Griffith University, PMB 50, Gold Coast Mail Center, Queensland 9726, Australia

Received: June 11, 2003; In Final Form: September 9, 2003

The effect of potential bias, light intensity, and the concentration of the photohole scavenger (glucose) on the photocurrent responses of the nanoporous TiO_2 film electrodes were investigated with the focus on the overall photoelectrocatalytic oxidation process. The electron transport in TiO_2 film was the rate-limiting step at low potential bias, while the interfacial reactions became rate-limiting step at high potential bias. A linear photocurrent/potential characteristic can be obtained within a wide range of applied potential bias. Within this linear range, the electrodes behave as a constant resistance rather than a variable resistance, which is unlike a photoelectrochemical process at a bulk semiconductor electrode. The resistance consists of two components: a variant component and an invariant component. The former is inversely proportional to maximum photocurrent, due to the free electron concentration change as a result of the consumption of photoholes through interfacial reaction. The hypothesis of the photoelectron and photohole separation being fulfilled through interfacial reaction was confirmed experimentally. The invariant component of the resistance is attributed to the sum of ohmic contact impedance at the ITO/TiO_2 interface and crystalline boundary impedance during electron migration under an electric field. A model for the overall photoelectrocatalytic oxidation process was proposed and explained based on the experimental results.

Introduction

The study and characterization of photocatalytic oxidative processes at photosensitive semiconductors by photoelectrochemical methods has several distinct advantages over systems that employ colloidal suspensions of semiconductor particles.[1−4] These include the fact that the oxidation half-reaction (at the working electrode) is physically separated from the reduction half-reaction (at the auxiliary electrode), which is in contrast to the colloidal suspension system where photooxidation and reduction reactions take place on the same particle.[5] This physical separation allows the reaction of interest (i.e., the photooxidation of organic substances) to be studied in isolation. For example, the rate or extent of reaction is determined only by the conditions and processes that occur (or are imposed) at the working electrode. This also allows simple quantification of the rate and extent of reaction by measurement of the photocurrent passed at the working electrode. Another advantage of the photoelectrochemical approach is that an applied potential bias is employed to minimize photoelectron−photohole recombination reactions as well as to manipulate aspects of the overall photocatalytic process. For example, the applied potential can be used to change the rate-determining steps of photocatalytic reactions,[1] which can facilitate elucidation of photocatalytic oxidation mechanisms.

In recent studies[1,2] we have shown that important kinetic information (e.g., rates of photocatalysis) and thermodynamic information (e.g., equilibrium adsorption constants) can be obtained in a simple, direct, and rapid manner by employing photoelectrochemical techniques. In these studies, thin TiO_2 nanoporous film electrodes (fabricated by immobilization of colloidal TiO_2 nanoparticles onto conducting ITO glass) were employed as the working electrode. While nanoporous film electrodes of this type have been used in other studies such as in potential assisted photocatalytic degradation of organic compounds[3,6−12] and in dye sensitized solar cell applications,[13−21] detailed studies on the exact nature of the photoelectrocatalytic processes that occur at these exist for conventional (bulk) semiconductor electrodes,[22−24] but not for particulate semiconductor electrodes, which are known to exhibit unique electrochemical and photoelectrochemical properties.[13]

One of the major differences between conventional semiconductor electrodes and particulate semiconductor electrodes is the nature of the energy bands (conduction and valence bands) that exist within each type of electrode. One of the most well described features of conventional semiconductor electrodes in photoelectrochemical experiments is the phenomenon of band bending within the space charge (or depletion) layer—particularly upon application of a potential bias.[22] In the case of particulate semiconductor electrodes, which contain aggregates of interconnected nanoparticles, the film electrode cannot sustain the development of a space charge layer.[13] Consequently, no clearly defined band bending is observed and the energy bands are essentially flat.[13] For this reason, the applied potential bias plays quite a different role in the particulate semiconductor electrode compared to conventional semiconductor electrodes. The exact nature of these differences has yet to be addressed in any detail in the literature when it comes to photocatalytic oxidation of organics at both types of electrodes.

As alluded to above, particulate TiO_2 semiconductor electrodes have been extensively employed and characterized in dye sensitized solar cell applications.[13−21] Issues such as electron transport in the film[19−23] and some fundamental semiconductive

* Corresponding author: Tel: +61-7-5552 8261. Fax: +61-7-55528607. E-mail: h.zhao@griffith.edu.au.

10.1021/jp0307349 CCC: $25.00
Published on Web 10/23/2003

characteristics of such films have been well investigated.[25−27] Although there are similarities between dye sensitized solar cell applications and the photoelectrochemical oxidation of organic substances at nanoporous TiO_2 film electrodes, there are some important differences. In dye sensitized cells, the electron injection into the conduction band of the film from the photoexcited dye is so overwhelmingly fast that charge separation can be easily realized and the recombination of photogenerated carriers is not a big concern. In this case, electron diffusion rather than electron migration under an electric field is believed to be the dominating mechanism of electron transport in the film.[19−21,23] In the case of photocatalytic oxidation of organics by direct absorption of light at TiO_2, both charge carriers are still on the TiO_2 surface. Effective charge separation can only be realized by removal of one of the charge carriers, and the overall efficiency depends on the effective removal of either charge carrier.[13] The mechanisms of how this happens and the processes that control charge carrier removal at nanoporous particulate electrodes have not been addressed in the literature.

The purpose of this study, therefore, is to shed light on the overall processes that occur during photoelectrocatalytic oxidation of organic material at TiO_2 nanoporous electrodes. Aspects such as which processes dominate or which processes are rate limiting under certain experimental conditions (which have not been reported for these electrodes) are addressed in detail. It is clear, for example, that application of a potential bias or changes in light intensity can cause changes in the overall rate of the photocatalytic reaction in these systems.[3,6−12] However, the mechanistic reasons for these observations and the extent to which each of these parameters affects the overall reaction rate have not been made clear at these electrodes. In this study, glucose, an effective photohole scavenger, was chosen as a model compound to study the effect of potential bias, light intensity, and concentration on the kinetics of photocatalytic oxidation. Detailed qualitative and quantitative descriptions of the overall photoelectrocatalytic processes that occur at nanoporous TiO_2 electrodes are presented.

Experimental Section

Materials. Conducting glass sheets (8−10 Ω/□, Delta Technologies Limited) were adopted as substrate for TiO_2 film coating. Titanium butoxide (97%, Aldrich), D-glucose (AnalaR, BDH), and sodium nitrate (99%, BDH) were used without further purification. All inorganic reagents used were of analytical grade unless otherwise stated. All solutions were prepared with water from a Millipore water purification system (Millipore Corp.). The solution pH was adjusted with nitric acid or sodium hydroxide solutions.

Preparation of Nanoporous TiO_2 Electrodes. The TiO_2 colloids were prepared by the hydrolysis of titanium butoxide according to the reported method.[28] The colloid obtained was then condensed to a final TiO_2 concentration of 60 g/L, to which carbowax was added before use. Upon pretreatment the slides were dip-coated in the colloid and ambient dried. Details of the electrode preparation have published elsewhere.[2] The thus-obtained electrodes were then fired in a muffle furnace at 500 °C for 30 min in air. The thickness of the film was ca. 1 μm measured with a surface profilometer (Alpha-step 200, Tencor Instruments). Characterized by X-ray diffraction (XRD) using a Philips PW1050 X-ray diffractometer, the film consists of mainly anatase phase with a negligible amount of brookite phase (less than 0.1% from fitting the XRD pattern). The morphology of the TiO_2 film electrodes was characterized by using a scanning electron microscope (SEM) (JSM-6400F, JEOL). Seen from the SEM image, the film is highly porous; the primary particles about 10−15 nm size still can be seen. The conducting glass sheets were mounted in a special electrode holder with 0.65 cm^2 left for contact with solution and for illumination, and with the rest sealed from contact with solution and from illumination.

Photoelectrochemical Measurements. The photoelectrochemical measurements were carried out in a photoelectrochemical cell with a quartz window in three-electrode mode, by which a saturated AgCl/Ag electrode was used as the reference electrode and a platinum mesh as the auxiliary electrode. The experiment setup was composed of a voltammograph (cv-27, BAS), an analog-to-digital converter (Maclab 400, AD Instruments), and a computer (7220/200, Macintosh) for sampling the potential and current signals. For illumination the light source was a 150 W xenon lamp housed with focusing lenses (HF-200w-95, Beijing Optical Instruments). For consistency the whole light unit was fixed on a rail track and the light intensity changes were made through altering the relative position of the electrolytic cell to the light source. Light intensity was measured with an UV-irradiance meter (UV-A, Instruments of Beijing Normal University). Prior to shining onto the electrode surface, the light beam passed a light filter (UG5, Avtronics Pty. Limited).

Results and Discussion

A photocatalytic reaction at semiconductor surfaces involves an interaction between photoholes and photohole scavengers. For a given system, the rate of the photocatalytic reaction is determined by the concentrations of both the photoholes and the scavenger—the former being determined by the intensity of the incident radiation and the latter being determined by the bulk concentration of the scavenger (i.e., glucose in this case). When the system involves a semiconductor electrode, the magnitude of the applied potential is also important in determining the kinetic characteristics of the system. Consequently, to fully characterize the photoelectrocatalytic processes that occur at nanoparticulate electrodes, we investigated the effect of varying all three of these variables, namely, applied potential, glucose concentration, and light intensity. This was achieved by performing slow linear sweep voltammetry at varying glucose concentrations and light intensities.

Influence of Applied Potential and Concentration. Figure 1 shows the voltammograms obtained at the TiO_2 particulate electrode, with or without UV illumination, in a 0.10 M $NaNO_3$ blank solution and various concentrations of glucose containing 0.10 M $NaNO_3$. As expected, it was found that without UV illumination, no measurable current was observed for both the blank and standard glucose solutions when the applied potential was more positive than −0.1 V. When the applied potential was below −0.1 V, a small cathodic current was observed for the blank solution (curve 16), which can be attributed to reduction processes at the underlying conducting glass (ITO) substrate. Curve 15 shows the photocurrent response of the electrode in the blank solution with UV illumination. In this case, the photocurrent increased with potential up to approximately −0.1 V before leveling off to a measurable anodic current of about 40 μA—this saturated current was due to the photocatalytic oxidation of water. In all other cases, the glucose $I-E$ responses increased linearly with potential before leveling off to saturated photocurrent values.

The effect of glucose concentration on the photocatalytic reaction rate can be seen in Figure 2, where the saturated

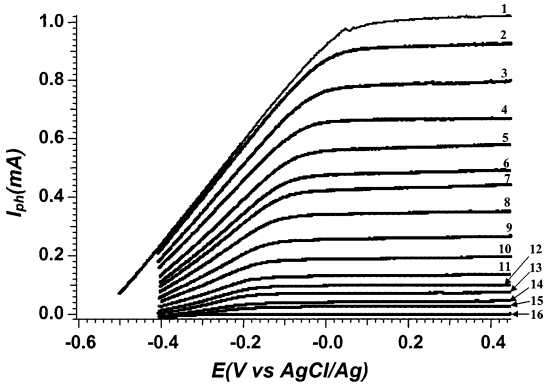

Figure 1. Voltammograms of TiO_2 film electrode obtained from a 0.1 M $NaNO_3$ blank and working solutions. The working solutions contain 0.1 M $NaNO_3$ and various concentrations of glucose. Scan rate 5 mV/s; light intensity 6.6 mW/cm^2. Curves 1−14 were obtained from the working solutions under UV illumination; the concentrations of glucose in turn were 0.45 M, 0.20 M, 0.10 M, 50 mM, 20 mM, 10 mM, 6 mM, 3 mM, 1.5 mM, 0.8 mM, 0.4 mM, 0.2 mM, 0.1 mM, and 0.02 mM. Curve 15 was obtained from the blank solution under UV illumination. Curve 16 was obtained from blank and working solutions without UV illumination.

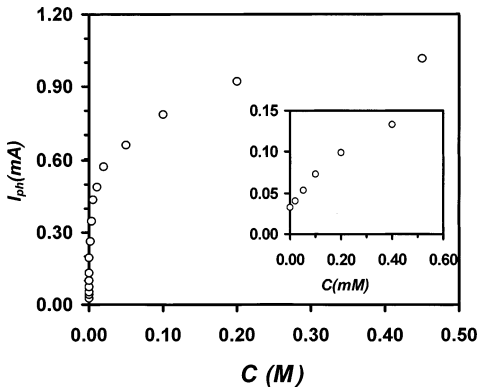

Figure 2. Dependence of saturation photocurrent on glucose concentration. Data derived from Figure 1. The inserted figure is the responses obtained from low concentration range.

photocurrents (I_{sph}) obtained from Figure 1 were plotted against concentrations. It was found that the I_{sph} values increased linearly with concentration up to 0.40 mM (see insert in Figure 2). Below this concentration, the rate of the photoelectrocatalytic process was limited by the mass transfer of glucose to the electrode surface (i.e., a diffusion-controlled process). At higher concentrations the I_{sph} values leveled off, at which point the reaction rate was limited by the film/solution interfacial reactions and, in particular, the photohole capture process, which dominates the overall reaction under these concentrations.

The curves shown in Figures 1 and 2 were qualitatively similar to those shown in our previous study on the photoelectrochemical oxidation of methanol.[1] Not surprisingly, therefore, treatment of the data according to Langmuir−Hinshelwood adsorption kinetics[1] confirms that the limitations in the reaction rates above 0.40 mM were due to the gradual saturation of glucose adsorption at the TiO_2 surface.

The most important feature of the $I-E$ data shown in Figure 1 was that, at all glucose concentrations, the photocurrent response increased linearly from the zero current potential before leveling out at higher potentials. In addition, the linear part of the curves extended to more positive potentials at higher glucose concentrations while the zero current potential was observed to shift to more negative potentials with an increase in concentration. This behavior is markedly different from what

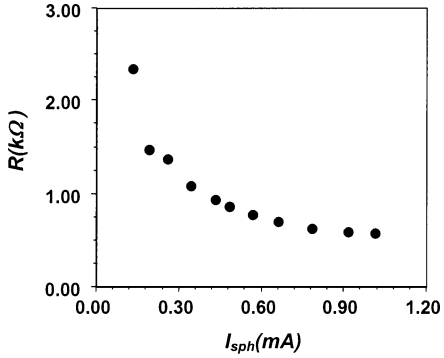

Figure 3. Relationship between resistance and saturation photocurrent in the photocurrent/potential linear region. Data derived from Figure 1.

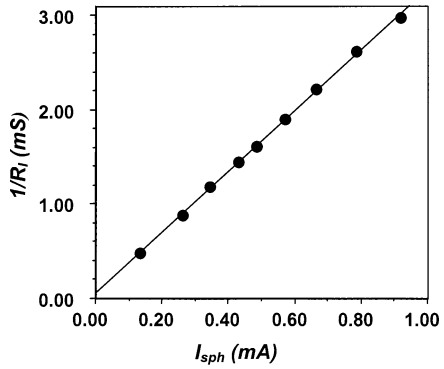

Figure 4. Inverse of variant part of resistance R_s against saturation photocurrent.

is observed at conventional (bulk) semiconductor electrodes in which a nonlinear (exponential) $I-E$ response is expected at potentials higher than the zero current potential.[23,24] In fact, the linear $I-E$ characteristic is one of the features of nanoparticulate electrodes that distinguish them from conventional semiconductor electrodes.

The rate-limiting process within the linear part of the curves in Figure 1 was electron transport within the TiO_2 film, and the system behaved like a pure resistance in its response to the potential change. The resistance values for each curve in Figure 1 can be calculated (according to Ohm's law), by dividing the potential change with the corresponding photocurrent change within the linear part of each curve. For a given light intensity, these resistances change with glucose concentration, which in turn determines the maximum reaction rate (expressed as I_{sph}). Plotting the resistance (R) against I_{sph} gives the hyperbolic curve shown in Figure 3. Computer curve fitting of the data shows that the $R-I_{sph}$ curve fits well with eq 1:

$$R = k/I_{sph} + R_0 \quad (1)$$

where $k = 310$ mA Ω, $R_0 = 245$ Ω, and both are constant for a given electrode and light intensity.

Equation 1 indicates that the total resistance can be divided into two parts: one is constant and independent of glucose concentration (R_0), and the other varies with maximum reaction rate as determined by different glucose concentrations ($R_I = k/I_{sph}$). The variable component of the resistance, R_I, can be obtained according to $R_I = R - R_0$. Plotting $1/R_I$ against I_{sph} gives a straight line as shown in Figure 4. Since $1/R_I$ represents the conductance, the conductance is directly proportional to I_{sph}. The conductance here is, in fact, the conductance of the TiO_2 film because the data used were obtained under conditions where the overall rate of reaction was controlled by electron transport

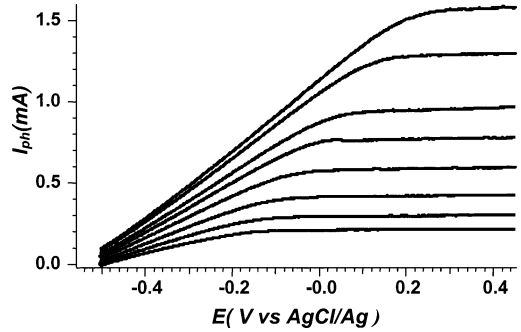

Figure 5. Voltammograms of electrode obtained from a solution containing 0.1 M $NaNO_3$ + 0.45 M glucose under illumination of different light intensities. Light intensity from top to bottom: 11.42. 10.11, 7.49, 6.10, 4.66, 3.26, 2.19, and 1.56 mW/cm^2.

in the TiO_2 film. Under these conditions, an increase in the glucose concentration (an effective photohole scavenger) resulted in a faster consumption of photoholes to produce higher electron concentration in the film. This phenomenon manifested itself in the experimental observation of a decrease in the resistance (or an increase in the conductivity) of the TiO_2 film. In other words, the liner relationship between the I_{sph} and film conductance implied that the surface reaction (which is concentration dependent) determined the electron concentration in the film, and that the migration of electrons under an electric field is directly proportional to the applied potential. The constant component of the resistance, R_0, likely reflects the sum of TiO_2 crystal boundary resistances and the resistances at the ITO/TiO_2 interface, which is an intrinsic property of the electrode.

Dependence of Photocurrent on Applied Potential and Light Intensity. Figure 5 shows the voltammograms obtained at the TiO_2 particulate electrode in a fixed concentration of photohole scavenger (0.45 M glucose in 0.1 M $NaNO_3$) under different illumination intensities. Under each given light intensity, the photocurrent response increased linearly with applied potential before leveling off. Both the saturation photocurrent and the potential range of the linear part of the $I-E$ curve increased as the light intensity was increased.

The linear $I-E$ relationship obtained again indicates that the electrode behaved markedly different from what would be expected at conventional (bulk) semiconductor electrodes. The pure resistor type behavior alluded to in the previous section again indicates that the rate of the reaction within the linear range was controlled by the electron transport in the TiO_2 film. The photocurrent (rate of reaction) observed in this part of the curve reflects how quickly the electrons in the semiconductor film can be removed by the applied potential. At a given light intensity, an increase in the applied potential leads to an increase in the electromotive force, which, in turn, leads to a proportional increase in the photocurrent (as expected by Ohm's law).

Figure 6 shows the relationship of the resistances obtained from the linear regions of the curves in Figure 5 (at different light intensities) versus I_{sph}. Again it was found that the resistance decreased with light intensity or with the maximum reaction rate (expressed as I_{sph}) in a hyperbolic manner. Computer curve fitting of the data revealed that the $R-I_{sph}$ curve fits eq 1 well with $k = 364$ mA Ω and $R_0 = 245$ Ω. This result again shows that a component of the total resistance is independent of light intensity or the maximum reaction rate. More importantly, the value of the constant resistance value obtained here was the same as the one obtained when the concentration of the glucose was varied. This provides strong

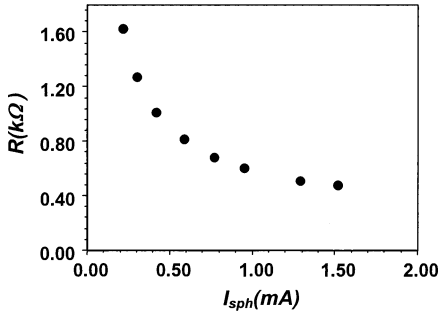

Figure 6. Relationship between resistance and saturation photocurrent in the photocurrent/potential linear region. Data derived from Figure 5.

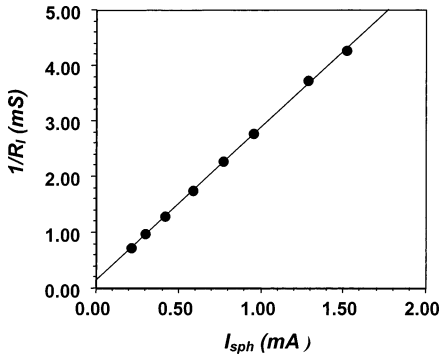

Figure 7. Inverse of variant part of resistance R_s against saturation photocurrent. Data derived from Figure 6.

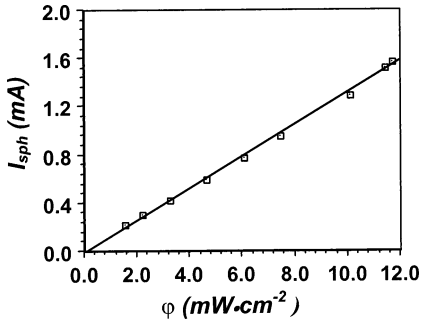

Figure 8. Saturation photocurrent dependence on light intensity. Data derived from Figure 5.

support for the previous argument that R_0 is an intrinsic property of the electrode. The variable component of the resistance, R_I, can be treated in the same way as for Figure 4 to give Figure 7. The result confirms that the conductivity of the film is directly proportional to the maximum reaction rate. At a particular glucose concentration, an increase in the light intensity led to an increase in the photohole concentration in the film. A higher photohole concentration made it easier for the photohole to be consumed by its scavenger (i.e., glucose), resulting in a decrease in the resistance (or increase in conductance) of the film with increased light intensity.

Another interesting feature about the curves in Figure 5 was the relationship between the saturated photocurrents (measured at +0.40 V) and the light intensity. In this region of the $I-E$ curves the rate-determining step was the interfacial reactions rather than the electron transport process in the film. Plotting the saturation photocurrent against the light intensity gives a straight line (see Figure 8). This linear dependence is indicative of a general assumption of photocatalytic process that the interfacial reaction with respect to surface bound photoholes is first order.[5] This result is in contrast to reported results

employing a TiO_2 colloidal suspension where a half-order dependence of the reaction rate on light intensity is often obtained.[5]

Applied Potential and the Maximum Reaction Rate. The results and subsequent data analysis presented in the above two sections focus on changes in film resistances (in the linear part of the $I-E$ curve) and how they are quantitatively related to the maximum reaction rate (as determined by glucose concentration). In this part, we complete the quantitative description of the $I-E$ curves, shown in Figures 1 and 5, by focusing on the saturated photocurrent values where the interfacial reaction rate was at maximum for a given glucose concentration and/or light intensity. In particular, we present an explanation why at a certain potential the photocurrent is saturated (maximum reaction rate) and why the potential is shifted with a change in glucose concentration (Figure 1) and light intensity (Figure 5).

At potentials where the saturated photocurrents were obtained, the maximum interfacial reaction rate was first-order with respect to photohole surface concentration and glucose surface concentration, respectively, as was demonstrated by the saturation photocurrent/glucose concentration relationship (Figure 2, insert) and the saturation photocurrent/light intensity relationship (Figure 8). The maximum interfacial reaction rate can therefore be expressed as

$$\text{rate}_m = k_1 C_{s,h} C_{s,glu} \tag{2}$$

where k_1 is a constant, $C_{s,h}$ is the photohole concentration at the TiO_2 surface, and $C_{s,glu}$ is the glucose concentration at the TiO_2 surface.

Since the saturation photocurrent is directly proportional to the maximum interfacial reaction rate, we have

$$I_{sph} = k_2 C_{s,h} C_{s,glu} \tag{3}$$

where I_{sph} is the saturation photocurrent and k_2 is a constant.

The maximum number of free electrons, N_{max}, in the TiO_2 film that are set free by the interfacial reactions at the maximum rate is proportional to I_{sph}

$$N_{max} = k_3 C_{s,h} C_{s,glu} \tag{4}$$

The photocurrent (I_{ph}) equals the numbers of electrons collected per unit time, and the magnitude of the photocurrent is determined by the saturation photocurrent and the efficiency of the electron collection, i.e.

$$I_{ph} = \alpha I_{sph} \tag{5}$$

where α is the electron collection coefficient and is defined as

$$\alpha = N_e/N_{max} \tag{6a}$$

where N_e is the number of electrons collected and is directly proportional to I_{ph}. According to these definitions, the electron collection coefficient in the photocurrent/potential linear region can be easily obtained:

$$\alpha = \Delta E/(k + R_0 k_2 C_{s,h} C_{s,glu}) \tag{6b}$$

where ΔE is the potential difference between the applied potential and the zero current potential; k is the slope of the curve in Figure 4 or 7 (see eq 1), which is a constant within the linear photocurrent range.

Equation 6b indicates that, from the zero current potential, α increased from 0 to 1 linearly with applied potential for a given set of light intensity and concentration. The maximum electron collection ($\alpha = 1$) or maximum rate of reaction can be achieved when

$$\Delta E = k + R_0 k_2 C_{s,h} C_{s,glu} \tag{7}$$

The rate of reaction will not be increased when the applied potential is beyond this point because k is no longer a constant. Equation 7 indicates that the magnitude of the potential difference, positive of the zero current potential (ΔE), required to achieve the maximum reaction rate is linearly dependent on both $C_{s,h}$ and $C_{s,glu}$. This can be seen in both Figures 1 and 5, where the potential at which the maximum reaction rate was achieved increased with both concentration (Figure 1) and light intensity (Figure 5).

The characteristics of the voltammograms of the TiO_2 film electrode in Figures 1 and 5 can be explained well by the above equations. The overall photoelectrocatalytic oxidation process at the nanoporous TiO_2 can be described clearly.

Further Discussions. The results and discussions presented above quantitatively characterize the $I-E$ responses at TiO_2 nanoporous film electrodes and demonstrate the differences in the overall photoelectrocatalytic behavior of these electrodes in comparison with conventional semiconductor electrodes. This section develops this concept further, in a qualitative sense by highlighting some of the fundamental differences between a particulate and a conventional semiconductor electrode. In addition, the differences between TiO_2 particulate film electrodes in solar cell applications and in their use in direct photoelectrocatalytic oxidation of organics are also addressed.

As pointed out in the Introduction, it is well-known that, unlike conventional semiconductor electrodes, particulate electrodes cannot sustain the development of a space charge layer and, consequently, the energy bands are almost flat.[13] For these reasons, the applied potential plays a quite different role in the particulate and the conventional semiconductor electrodes. With a conventional semiconductor electrode, the main function of the applied potential is to regulate the band bending across the space charge region in order to, typically, minimize electron−hole recombination processes. In addition, where necessary, the applied potential bias can accelerate the interfacial electron transfer process. In the case of a particulate semiconductor electrode, the spatial separation of photogenerated hole−electron pairs can be achieved only by removal of photoholes through interfacial reactions since there is no band bending. The applied potential serves the function of collecting the free electrons made available by the interfacial reactions. In other words, the applied potential simply assists in the removal of the free electrons. It cannot serve the purpose of controlling the interfacial reaction, and instead the interfacial reaction rate controls the free electron concentration in the film. This fundamental difference between the two electrode types is demonstrated in Figures 4 and 7, where the conductance of the film changes linearly with the maximum reaction rate, which is determined by glucose concentration and light intensity. Under given conditions of light intensity and glucose concentration, the maximum interfacial reaction rate is fixed; so is the free electron concentration in the film. Application of the potential bias serves the function of facilitating the electron transport in the film that makes the overall reaction rate swing between zero (at the zero current potential) and the maximum, where $\Delta E = k + R_0 k_2 C_{s,h} C_{s,glu}$.

As pointed out in previous sections, close inspection of Figures 1 and 5 reveals that the zero current potential changes slightly with changes in both scavenger (glucose) concentrations and light intensity at low glucose concentration and low light intensity, but approaches a constant value at higher glucose

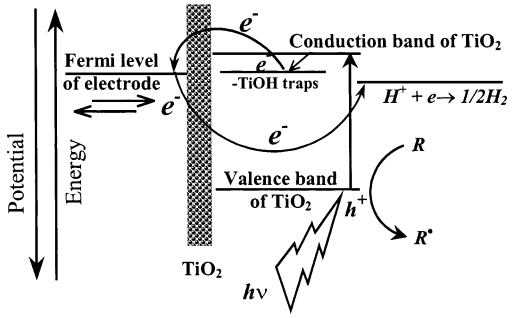

Figure 9. Schematic of the relative energetics of the electrode.

concentration. The shift of zero current potential at low glucose concentration can be attributed to the negative contribution of the cathodic current of direct electrochemical reduction at the underlying ITO glass electrode. At higher glucose concentration and light intensity, the constant zero current potential should reflect the energy band position of the electron band. It is noticed that the constant zero current potential (−0.55 V vs Ag/AgCl at pH ca. 6.0) is higher than the flat band potential expected for anatase TiO_2 semiconductor (ca. −0.72 V vs Ag/AgCl).[29] Therefore, this zero current potential is most likely the subband position of electron traps inherent to the large surface area of TiO_2 nanoparticles.[5,30,31]

Given this, the energy level diagram for the system can be represented schematically as shown in Figure 9. As illustrated in the figure, the Fermi level of the conducting ITO substrate is controlled by the applied potential. As the potential is lower than the water reduction potential, the pure electrochemical reduction takes place at the underlying ITO substrate, generating a cathodic current. Upon illumination, photoelectrons are generated and are subsequently trapped by the TiO_2 surface groups. Once the applied potential is positive of the electron trap potential, a flow of electrons from the trap band to the conducting substrate occurs and an anodic current is generated. The carrier concentration in the film is extremely low when there is no UV illumination; therefore, no anodic current can be generated even when the electrode potential is much more positive than the trap band potential. Under UV illumination, when the potential is above the zero current potential or trap band potential and the photoholes are removed by the interfacial reactions, surface photoelectrons flow through the film to the conducting ITO substrate. Meanwhile, at the bare/exposed ITO sites the direct electrochemical reduction reaction still occurs, and as a result, the total current obtained is the sum of the reduction and oxidation processes. Consequently, the zero current potential changes slightly. However, at higher glucose concentration and higher light intensity, since the available free electron concentration in the trap band is much higher and the reduction current is negligible in comparison with the anodic current generated from the oxidation process, the zero current potential approaches the trap band potential.

Some have argued that there was no electric field across the film due to the low conductivity of TiO_2 film and the screening effect by penetrating ions.[32] Apparently this argument cannot explain the linear dependence of photocurrent on applied potential as demonstrated in this work. For a thin TiO_2 film about 1 μm which is close to the UV light penetrating range the conductance can be greatly increased under illumination.[33] From the film resistance study in the above sections, it has been found that under illumination the resistance in the film is dramatically decreased as long as there are enough photohole scavengers at the TiO_2 surface. Due to the great difference in mobility between ions in pores and the free electrons in film, the screening effect can be neglected and an electric field can be established inside the film.

The main application area for TiO_2 particulate film electrodes to date has been in dye sensitized solar cell developments, where considerable attention has been given to electron transport mechanisms within the film. Many believe the driving force for electron transport in theTiO_2 film is the electron concentration gradient in the film.[33−35] For dye sensitized TiO_2 porous film this may be true because the electrons typically exist as free electrons in the film due to the extremely high electron injection rate compared with the relatively slow electron−hole recombination process.[13,14,36] As a result, even though there is no external applied electric field, the free electrons can still diffuse to the collecting electrodes with little chance for recombination to occur. In our case electrons can only be set free when the photoholes are removed from the surface (by the interfacial reaction). In addition, the rate of photohole consumption is not overwhelmingly higher than the rate of electron−hole recombination, and the buildup of free electrons will significantly increase the rate of photoelectron/photohole recombination. Therefore, the electric field in the film (induced by the applied potential) plays an important role in the overall photocatalytic oxidation reaction. This can be demonstrated by results from both Figure 1 and Figure 5, where the higher the overall interfacial reaction rate the larger the potential drop (applied potential) needed to drive the electrons out of the film. This is fundamentally different from the dye sensitized solar cell applications of TiO_2 particulate film electrodes.

Conclusions

The overall photoelectrocatalytic oxidation process at nanoporous TiO_2 film electrodes has been quantitatively and qualitatively characterized using glucose as a model photohole scavenger. At high glucose concentrations the photocurrent increases linearly with potential positive of the zero current potential. This behavior is peculiar to particulate semiconductor electrodes and is indicative of the absence of band bending in these systems. Altering light intensity as well as surface glucose concentration can change the maximum photocurrent or reaction rate. This saturated photocurrent (at high potential bias) linearly increases with light intensity and glucose surface coverage, which confirms that the heterogeneous photocatalytic reaction is a bimolecular reaction.

Investigations of the change of potential-dependent reaction rate with changing glucose concentrations and changing light intensities revealed the existence of two types of resistances—a variable component and a nonvariable component. The variable component of the resistance was shown to be inversely proportional to the maximum photocurrent or maximum rate of reaction, indicating that the interfacial reaction rate determines the concentration of free electrons in the film. The invariable part of the resistance is attributed to the intrinsic resistance of the electrode, resulting from the grain boundary resistances and the ohmic contact at the ITO/TiO_2 interface. The manner in which the applied potential influenced the photocurrent in the linear part of the $I-E$ curves confirmed that electron transport in the film is determined by migration under an electric field rather than by diffusion. An important role of applied potential bias is to prevent the buildup of free electrons released by photohole surface capture reaction, which, in turn, minimizes the recombination of photoelectrons and photoholes.

References and Notes

(1) Jiang, D.; Zhao, H.; Jia, Z.; Cao, J.; John, R. *J. Photochem. Photobiol. A: Chem.* **2001**, *144*, 197−204.

(2) Jiang, D.; Zhao, H.; Zhang, S.; John, R.; Will, G. D. *J. Photochem. Photobiol. A: Chem.* **2003**, *156*, 201−206.
(3) Butterfield, I. M.; Christensen, P. A.; Hamnett, A.; Shaw, K. E.; Walker, G. M.; Walker, S. A. *J. Appl. Electrochem.* **1997**, *27*, 385−395.
(4) Mandelbaum, P.; Regazzoni, A. E.; Blesa, M. A.; Bilmes;, S. A. *J. Phys. Chem. B* **1999**, *103*, 5505.
(5) Hoffmann, M. R.; Martin, S. T.; Choi, W.; Bahnemann, D. W. *Chem. Rev.* **1995**, *95*, 69−96.
(6) Vinodgopal, K.; Hotchandani, S.; Kamat, P. V. *J. Phys. Chem. B* **1993**, *97*, 9040−9044.
(7) Vinodgopal, K.; Stafford, U.; Gray, K. A.; Kamat, P. V. *J. Phys. Chem. B* **1994**, *98*, 6797−6803.
(8) Calvo, M. E.; Candal, R. J.; Bilmes, S. A. *Environ. Sci. Technol.* **2001**, *35*, 4132−4138.
(9) Vinodgopal, K.; Bedja, I.; Kamat, P. V. *Chem. Mater.* **1996**, *8*, 2180−2187.
(10) Kim, D. H.; Anderson, M. A. *Environ. Sci. Technol.* **1994**, *28*, 479−483.
(11) Mandelbaum, P.; Bilmes, S. A.; Regazzoni, A. E.; Blesa, M. A. *Solar Energy* **1998**, *65*, 75−80.
(12) Wahl, A.; Ulmann, M.; Carroy, A.; Augustynski, J. *J. Chem. Soc., Chem. Commun.* **1994**, 2277−2278.
(13) Hagfeld, A.; Gratzel, M. *Chem. Rev.* **1995**, *95*, 49−68.
(14) Cahen, D.; Hodes, G.; Gratzel, M.; Guillemoles, J. F.; Riess, I. *J. Phys. Chem. B* **2000**, *104*, 2053−2059.
(15) Huang, S. Y.; Schlichthorl, G.; Nozik, A. J.; Gratzel, M.; Frank, A. J. *J. Phys. Chem. B* **1997**, *101*, 2576−2582.
(16) Park, N.-G.; Schlichthorl, G.; van de Lagemaat, J.; Cheong, H. M.; Mascarenhas, A.; Frank, A. J. *J. Phys. Chem. B* **1999**, *103*, 3308−3314.
(17) Park, N. G.; van de Lagemaat, J.; Frank, A. J. *J. Phys. Chem. B* **2000**, *104*, 8989−8994.
(18) Bach, U.; Tachibana, Y.; Moser, J.-E.; Haque, S. A.; Durrant, J. R.; Gratzel, M.; Klug, D. R. *J. Am. Chem. Soc.* **1999**, *121*, 7445−7446.
(19) Kuciauskas, D.; Freund, M. S.; Gray, H. B.; Winkler, J. R.; Lewis, N. S. *J. Phys. Chem. B* **2001**, *105*, 392−403.
(20) Schlichthorl, G.; Huang, S. Y.; Sprague, J.; Frank, A. J. *J. Phys. Chem. B* **1997**, *101*, 8141−8155.
(21) Trupke, T.; Wurfel, P.; Uhlendorf, I. *J. Phys. Chem. B* **2000**, *104*, 11484−11488.
(22) Morrison, S. R. *Electrochemistry at Semiconductor and Oxidized Metal Electrodes*; Plenum Press: New York, 1980.
(23) Butler, M. A. *J. Appl. Phys.* **1977**, *48*, 1914−1920.
(24) Ginley, D. S.; Butler, M. A. *J. Appl. Phys.* **1977**, *48*, 2019−2021.
(25) Yan, S. G.; Hupp, J. T. *J. Phys. Chem. B* **1996**, *100*, 6867−6870.
(26) Lyon, L. A.; Hupp, J. T. *J. Phys. Chem. B* **1999**, *103*, 4623−4628.
(27) Zaban, A.; Ferrere, S.; Gregg, B. A. *J. Phys. Chem.* **1998**, *102*, 452−460.
(28) Barbe, C. J.; Arendse, F.; Comte, P.; Jirousek, M.; Lenzmann, F.; Shklover, V.; Gratzel, M. *J. Am. Ceram. Soc.* **1997**, *80*, 3157−3171.
(29) Kavan, L.; Gratzel, M.; Gilbert, S. E.; Klemenz, C.; Scheel, H. J. *J. Am. Chem. Soc.* **1996**, *118*, 6716−6723.
(30) Szczepankiewicz, S. H.; Colussi, A. J.; Hoffmann, M. *J. Phys. Chem. B* **2000**, *104*, 9842−9850.
(31) Wang, H.; He, J.; Boschloo, G.; Lindstrom, H.; Hagfedt, A.; Lindquist, S.-e. *J. Phys. Chem. B* **2001**, *105*, 2529−2533.
(32) Zaban, A.; Meier, A.; Gregg, B. A. *J. Phys. Chem. B* **1997**, *101*, 7985−7990.
(33) de Jough, P. E.; Vanmaekelbergh, D. *J. Phys. Chem. B* **1997**, *101*, 2716−2722.
(34) Wahl, A.; Augustynski, J. *J. Phys. Chem. B* **1998**, *102*, 7820−7828.
(35) van de Lagemaat, J.; Frank, A. J. *J. Phys. Chem.* **2001**, *105*, 11194−11205.
(36) Salafsky, J. S.; Lubberhuizen, W. H.; van Faassen, E.; Schropp, R. E. I. *J. Phys. Chem. B* **1998**, *102*, 766−769.